AGU PUBLICATIONS

Water Resources Research

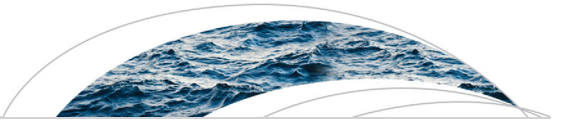

RESEARCH ARTICLE
10.1002/2016WR019937

Transverse and longitudinal mixing in real emergent vegetation at low velocities

F. Sonnenwald[1], J. R. Hart[2], P. West[2], V. R. Stovin[1], and I. Guymer[2]

[1]Department of Civil and Structural Engineering, The University of Sheffield, Sheffield, UK, [2]School of Engineering, University of Warwick, Coventry, UK

Key Points:
- A new lab data set describes transverse and longitudinal dispersion in real emergent vegetation
- New and existing data have been compared with models for predicting dispersion
- Current dispersion models relying on mean stem diameter do not describe real vegetation well

Correspondence to:
F. Sonnenwald,
f.sonnenwald@sheffield.ac.uk

Citation:
Sonnenwald, F., J. R. Hart, P. West, V. R. Stovin, and I. Guymer (2017), Transverse and longitudinal mixing in real emergent vegetation at low velocities, *Water Resour. Res.*, *53*, 961–978, doi:10.1002/2016WR019937.

Received 13 OCT 2016
Accepted 3 JAN 2017
Accepted article online 8 JAN 2017
Published online 31 JAN 2017

Abstract Understanding solute mixing within real vegetation is critical to predicting and evaluating the performance of engineered natural systems such as storm water ponds. For the first time, mixing has been quantified through simultaneous laboratory measurements of transverse and longitudinal dispersion within artificial and real emergent vegetation. Dispersion coefficients derived from a routing solution to the 2-D Advection Dispersion Equation (ADE) are presented that compare the effects of vegetation type (artificial, *Typha latifolia* or *Carex acutiformis*) and growth season (winter or summer). The new experimental dispersion coefficients are plotted with the experimental values from other studies and used to review existing mixing models for emergent vegetation. The existing mixing models fail to predict the observed mixing within natural vegetation, particularly for transverse dispersion, reflecting the complexity of processes associated with the heterogeneous nature of real vegetation. Observed stem diameter distributions are utilized to highlight the sensitivity of existing models to this key length-scale descriptor, leading to a recommendation that future models intended for application to real vegetation should be based on probabilistic descriptions of both stem diameters and stem spacings.

1. Introduction

Natural and engineered environmental systems such as wetlands or storm water ponds typically contain vegetation and are often designed specifically to treat pollutants [*Shilton*, 2000]. To protect natural systems and design effective engineered systems, it is necessary to quantify the impact of aquatic vegetation on solute mixing. Understanding mixing in these flows is relevant to a number of other environmental applications, e.g., seed dispersal [*Merritt and Wohl*, 2002] or nutrient transport [*Nishihara and Terada*, 2010].

Quantifying the impact of vegetation on hydroenvironmental systems is a challenging task. Vegetation is characterized by small leaves and slightly larger stems, located in bodies of water much larger than a single plant, resulting in a multiscale problem that cannot easily be directly modeled. An approach that spatially averages the effects of the vegetation, i.e., a bulk mixing characterization, is generally preferred [e.g., *Nepf*, 1999].

The mixing of a solute can be described by the temporally and spatially averaged advection-dispersion equation (ADE):

$$\frac{\partial C}{\partial t}+u\frac{\partial C}{\partial x}+v\frac{\partial C}{\partial y}+w\frac{\partial C}{\partial z}=D_x\frac{\partial^2 C}{\partial x^2}+D_y\frac{\partial^2 C}{\partial y^2}+D_z\frac{\partial^2 C}{\partial z^2} \quad (1)$$

where C is the concentration of a conservative solute (e.g., a pollutant or tracer), u, v, and w are the velocity in the x (stream-wise), y (transverse), and z (vertical) directions, t is time, and D_x, D_y, and D_z are the dispersion coefficients in each direction [*Fischer et al.*, 1979]. The velocity terms describe the advection of the solute. The dispersion coefficients aggregate all the mixing processes that may affect the solute within the volume of interest. These include instantaneous velocity fluctuations, leading to turbulent diffusion, and velocity field heterogeneity, producing mechanical dispersion.

The aim of this paper is to present and interpret new laboratory data that quantifies transverse and longitudinal mixing for vegetation types and flow velocities that are typical for engineered storm water ponds.

2. Previous Research

2.1. Experimental Dispersion Studies

Previous experimental studies aimed at determining dispersion coefficients within real emergent vegetation include: *Nepf* [1999], *Huang et al*. [2008], *Lightbody and Nepf* [2006b], *Wadzuk and Burke* [2006], *Shucksmith et al*. [2010], and *Erqing et al*. [2010]. *Nepf* [1999] also studied artificial vegetation, along with *Nepf et al*. [1997a, 1997b], *Serra et al*. [2004], *Tanino and Nepf* [2008a], *White and Nepf* [2003], and *Lightbody and Nepf* [2006a]. The majority of these studies either investigated longitudinal or transverse mixing, although *Nepf et al*. [1997b] and *Huang et al*. [2008] also evaluated vertical mixing. The data available from these studies are summarized in Table 1.

While the data sets of these studies provide valuable insights into dispersion within vegetation, the specific physical characteristics of individual plant species imply that different dispersion processes will dominate, and that the values of longitudinal and transverse dispersion parameters obtained in previous investigations may not be transferable to different plant species. The physical characteristics of the plants are also expected to change over time as a result of their seasonal growth cycles. The focus of the current research is on characterizing dispersion for vegetation types typically associated with storm water ponds, specifically *Carex acutiformis* and *Typha latifolia*, with the *Typha* being considered at two different growth stages. As velocities within storm water ponds are typically very low, the present study focuses on obtaining experimental data at velocities ≤ 0.02 m/s. Generalization of the observed dispersion characteristics may be achieved through the development of process-based conceptual models that aim to predict dispersion coefficients from measurable plant physical characteristics. Relevant modeling approaches are described below.

2.2. Mixing Models Within Emergent Vegetation

2.2.1. Transverse Mixing Models

Nepf et al. [1997b] and *Nepf* [1999] proposed a model to estimate transverse dispersion within emergent vegetation due to two processes. First, energy dissipation from the stem drag force, due to the wake structure formation, was assumed to appear as turbulent kinetic energy and termed "turbulent" diffusion. The validity of this assumption is discussed in more detail in *Nikora* [2000] and in the subsequent reply by *Nepf* [2000]. Second, the individual flow paths imposed by the tortuosity caused by the physical obstruction of the stems, was termed "mechanical" diffusion. *Nepf* [1999] proposed that D_y may be determined from:

$$\frac{D_y}{Ud} = \alpha[C_D ad]^{1/3} + \left[\frac{\beta^2}{2}\right] ad \tag{2}$$

where U is the spatial and temporal mean longitudinal (i.e., stream-wise) velocity, d is stem diameter, C_D is mean bulk drag coefficient, a is frontal facing area per unit volume, and α and β are first-order scaling coefficients. ad is a measure of density. The first term on the right represents mixing resulting from drag force energy dissipation, and the second term flow path tortuosity. *Nepf* [1999] identified a best fit value of $\alpha = 0.81 \pm 0.09$ for experimental results and assumed a value of $\beta = 1$.

Table 1. Data Sets Characterizing Dispersion in Emergent Vegetation From Other Studies

Type	Study Outline[a]	Data Collected	Stem Density N (stems/m^2)	Stem Diameter d (m)	Frontal Facing Area a (m^{-1})	Solid Volume Fraction ϕ (–)	Stem Reynolds Re_d (–)	Reference
Random artificial	CL	D_y, D_z	200–2000	0.006–0.012	1.3–11.3[b]	0.006–0.053	190–1800[b]	*Nepf et al*. [1997b]
Random artificial	CL	D_y	200-2000	0.0064	1.2–10.5	0.006–0.053	60–2000	*Nepf* [1999]
Spartina alterniflora	CF	D_y	96–370	0.0069 ± 0.0003	2.1–8.2	0.011–0.044[b]	200–600	*Nepf* [1999]
Random artificial	CL	D_y	130–450[b]	0.010	12.6–44.7[b]	0.010–0.035	10–100	*Serra et al*. [2004]
Phragmites australis	CF	D_y	180–560[b]	0.015 ± 0.011	2.7–8.5[b]	0.033–0.102	59–95	*Wadzuk and Burke* [2006]
Random artificial	CL	D_y	350–12,380[b]	0.006	2.0–69.3[b]	0.01–0.35	67–390	*Tanino and Nepf* [2008a]
Staggered artificial	CL	D_x	280–1700	0.006	2.12–11.7[b]	0.01–0.055	174–444[b]	*Nepf et al*. [1997a]
Random artificial	PL	D_x	317–2001[b]	0.0064	2.0–12.8[b]	0.01–0.064[b]	65–650	*White and Nepf* [2003]
Multispecies mix	PF	D_x, D_z	280–4460[b]	0.001–0.1	1.7–5.8	0.002–0.022[b]	18–272[b]	*Huang et al*. [2008]
Carex	PL	D_x	125–1042[b]	0.005–0.015	0.25–1.5[b]	0.002–0.059	2446–8442[b]	*Shucksmith et al*. [2010]
Phragmites australis	PL	D_x	300–333	0.003	0.89–1.0[b]	0.0021–0.0024	512–724[b]	*Shucksmith et al*. [2010]

[a](C)ontinuous or (P)ulse injection, (L)aboratory or (F)ield measurement.
[b]Estimated values when value not presented within reference.

Serra et al. [2004] proposed a modification of equation (2). Instead of *ad* they related mixing due to drag force energy dissipation and flow path tortuosity to the ratio of stem diameter to mean spacing between stems, *s*, giving:

$$\frac{D_y}{Ud}=\alpha\left[C_D\left(\frac{d}{s}\right)^2\right]^{1/3}+\left(\frac{\beta^2}{2}\right)\left(\frac{d}{s}\right)^2 \tag{3}$$

Based on relating drag force to a velocity deficit that encourages transverse mixing, *Serra et al*. [2004] suggested that:

$$\frac{D_y}{Ud}=\beta_s C_D\frac{d}{s} \tag{4}$$

where β_s is another dimensionless constant. Assuming cylindrical stems, *Serra et al*. [2004] derived $ad=G(d/s)^2$ for a random array of vegetation, with $G\approx 3.4$. It is evident that equations (2) and (3) are functionally equivalent, although α and β will have different absolute values. *Serra et al*. [2004] obtained values of $\beta_s C_D$ between 1 and 4, and this range of values provides comparable predictions to equation (2).

Tanino and Nepf [2008a] introduced a new model to estimate transverse dispersion based on *Nepf* [1999] to better describe the transition between drag force energy dissipation and flow path tortuosity dominated dispersion:

$$\frac{D_y}{Ud}=\gamma_1\frac{4}{\pi}\phi\left\langle\frac{\sqrt{k_t}}{U}\right\rangle P_{s_{nc}>r*}\frac{\langle s_n^2\rangle_{s_{nc}>r*}}{d^2}+\gamma_2 P_{s_{nc}<5d}\frac{\pi}{4096}\left(\frac{d^2}{k_\perp}\right)^{\frac{3}{2}}\frac{1-\phi}{\phi^2} \tag{5}$$

where ϕ is the solid volume fraction, k_t is the turbulent kinetic energy, $P_{s_{nc}>r*}$ is the probability the nearest stem is further than $r*$, $r*$ is the minimum distance between stems necessary to contribute to lateral mixing (assumed to be equivalent to $0.5d$), s_n is the distance between stems, s_{nc} is the center-to-center distance between stems, $P_{s_{nc}<5d}$ is the probability the nearest stem is located within $5d$, $k_\perp$ is the permeability in the direction of flow, and γ_1 and γ_2 are scaling constants with values of 4.0 and 0.34 as determined by least squares fitting to laboratory data. Again, the first term on the right represents mixing due to drag force energy dissipation and the second flow path tortuosity. *Tanino and Nepf* [2008a] provided expressions for all of the parameters in terms of ϕ, assuming a random array of cylinders. Therefore, the *Nepf* [1999] and *Tanino and Nepf* [2008a] models are effectively dependent on the same term (ϕ or ad). Both models also share the same semiempirical limitation of requiring best fit values (α, β, γ_1, and γ_2). It should also be noted that these models all assume a single, mean, value of stem diameter.

Nepf [2012] suggested that the models estimating mixing due to drag force energy dissipation and flow path tortuosity may be simplified depending on solid volume fraction, ϕ. When $\phi<0.1$ drag force energy dissipation dominates and $D_y(Ud)^{-1}=0.2$, and when $\phi\geq 0.1$ flow path tortuosity dominates and $D_y(Ud)^{-1}=ad=4\pi^{-1}\phi\approx\phi$.

2.2.2. Longitudinal Mixing Models

White and Nepf [2003] suggested that longitudinal dispersion in emergent vegetation is primarily due to vortex trapping ($D_{x,t}$) and stem-scale secondary wake dispersion ($D_{x,s}$). In vortex trapping, particles are entrained temporarily in the eddies formed behind stems. In secondary wake dispersion, particles travel between areas of lower velocity behind stems and higher velocity between stems, resulting in differential longitudinal advection. The expressions for dispersion due to vortex trapping and secondary wake dispersion are:

$$\frac{D_{x,t}}{Ud}=\frac{\beta_w\kappa_w}{St}ad \tag{6}$$

and

$$\frac{D_{x,s}}{Ud}=\frac{\gamma_w}{8\sqrt{ad}}\sqrt{C_D^3 adRe_t}\sqrt{\frac{Sc_t}{Sc_t+1}} \tag{7}$$

where β_w is a constant of proportionality describing the residence time in stem wakes (dependent on stem Reynolds number, Re_d), κ_w describes the wake-trapping zone (fraction of the volume with stem wakes, also

dependent on Re_d), St is the Strouhal number describing the oscillation of the vortices, γ_w is an incomplete gamma function, $Re_t = Ud(v_t + v)^{-1}$ is the turbulent Reynolds number, v_t is the turbulent viscosity, v is the molecular viscosity, and Sc_t is the turbulent Schmidt number. *Lightbody and Nepf* [2006b] simplified the secondary wake dispersion model (Equation 7) for $\phi < 0.1$ to:

$$\frac{D_{x,s}}{Ud} = \frac{1}{2} C_D^{3/2} \tag{8}$$

and for $\phi \geq 0.1$, *Murphy* [2006] proposed:

$$\frac{D_{x,s}}{Ud} = 5ad \tag{9}$$

Nepf et al. [1997a] and *Lightbody and Nepf* [2006a, 2006b] relate longitudinal dispersion to vertical dispersion, following the classic triple integral [*Fischer et al*., 1979]. *Lightbody and Nepf* [2006a, 2006b] suggest that vertical variations in longitudinal velocity, generated by vertically heterogeneous plant morphology, are responsible for a large portion of longitudinal dispersion within vegetation.

3. Methodology

3.1. Laboratory Setup

Controlled laboratory tests were conducted to simulate low velocity flow through uniform emergent vegetation in a 24 m long by 1 m wide recirculating flume with a horizontal bed. The experimental setup is shown in Figure 1. Channel discharge was maintained by a pump that fed water directly into the channel inlet after a flow expander. Two sets of flow straighteners, a plate drilled with an array of 0.05 m holes and an array of 0.005 m diameter tubes 0.05 m long, were positioned 0.2 and 0.5 m downstream of the inlet aligned in the direction of flow. Flow depth was controlled with a tail-gate located at the channel outlet and measured using a Vernier gauge, maintaining a fixed depth of 0.15 m within the test section.

Rhodamine 6G fluorescent dye was used to investigate solute transport through vegetation. Vertical line source injections were made at the channel center 12 m downstream from the flow straighteners using a copper pipe with 0.0008 m diameter holes at 0.01 m intervals. The pipe was connected to a constant-head tank located directly above the flume.

The flume was fitted with a 2-D laser induced fluorescence (LIF) system to measure temporal and transverse variations in dye concentration at two locations 1 and 2 m downstream from the injection point. To fluoresce the dye, 200 mW green lasers ($\lambda = 532$ nm) were installed on the side of the flume perpendicular to the flow at middepth. Observation windows (each 0.1 m wide) were installed across the vegetation bed at the measurement locations and digital cameras fitted below the flume looking up and capturing the full width of the channel and laser beam. Concentration records were captured at 5 Hz as a sequence of 1280 $\times$ 1024 8-bit grey-scale images. The entire flume was covered in black-painted wooden boards to minimize background interference from ambient lighting.

A calibration between pixel intensity and concentration was made simultaneously for both measurement locations. A short section of the flume containing the laser windows was isolated from the rest of the flume

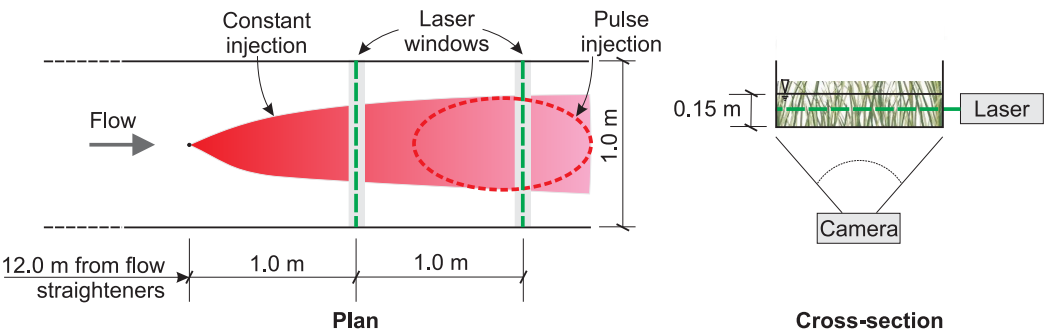

Figure 1. Schematic of laboratory flume and measurement system.

with baffles and a range of measurements of known Rhodamine 6G concentrations was taken with known laser powers. The calibration measurements were used in accordance with the Beer-Lambert law to obtain best fit values of the attenuation (α_w) and extinction (ϵ_0) coefficients of Rhodamine 6G, as well as best fit values ξ and ζ describing the relationship between pixel intensity and concentration [*West*, 2016]. To calibrate a recorded profile, a pixel-by-pixel decay model [*Ferrier et al*., 1993] was then applied, in which concentration measured at a pixel depends on both pixel intensity and concentration of the previous pixel:

$$P_{n+1}=P\exp\left(-\sum_{i=0}^{n}(\alpha_w+\epsilon_0 C_i)\Delta y\right) \tag{10}$$

where P is the laser power before entering the flume, P_{n+1} is the power in the pixel at location $n+1$ from the laser, C_i is the concentration in the pixel at location i, $C_i=(I_i P_{i-1}^{-1}-\zeta)\xi^{-1}$, I_i is the pixel intensity at i, P_{i-1} is the laser power at the previous pixel, and Δy is the width of a pixel. At $i=0$, $P_{i-1}=P$.

The artificial vegetation was installed between 10 and 15.2 m downstream from the flow straighteners. Real vegetation was installed between 7 and 17 m. The vegetation was omitted above each observation window to ensure a clear image and for taking measurements of velocity. The real vegetation was cropped to a depth of 0.25 m, permitting access to the flow and to allow the laser blackout covers to be fitted. Profiles of instantaneous vertical and transverse velocity were measured with Met-Flow UVP-DUO velocity probes to verify uniform velocity fields. Velocity data were despiked according to *Goring and Nikora* [2002].

Two injection methods were employed. Primarily, 5 s pulse injections were made, with 10 repetitions to capture the spread of the data. Second, continuous dye injections were made for 10 min to simulate steady state conditions for one artificial and two real vegetation experiments. The vertical line source eliminated the observational effects of vertical dispersion. The continuous injection eliminated the observational effects of longitudinal dispersion, while the pulse injection allowed both transverse and longitudinal mixing to be observed. The experimental setup is explained in more detail in *West* [2016]. This experimental setup allowed D_x and D_y to be determined simultaneously from a single pulse injection for the first time. Simultaneous measurements simplify the practical constraints of measuring dispersion, reducing flume sump dye saturation due to a continuous injection and time spent on experimental procedures, and also ensure that the two measurements are linked to the exact same flow conditions and vegetation arrangement.

3.2. Experimental Configurations

Experimental dispersion data were collected for two densities of artificial vegetation (AV) and three types of real vegetation (*Carex acutiformis*, winter *Typha latifolia*, and summer *Typha latifolia*), shown in Figure 2 [*Hart et al*., 2016]. Figure 2c also shows the laser line sources used to illuminate the flow at the two measurement windows. The artificial vegetation consisted of 0.004 m diameter drinking straws at two densities of a repeating regular hexagonal grid. The high-density variant had a density of 1594 stems/m^2 with a center-to-center stem spacing of 0.025 m transversely and 0.0125 m longitudinally, with every other row being offset by one stem (inset Figure 2a). The low-density artificial vegetation was generated by removing 3 out of 4 straws, thereby multiplying these dimensions by two.

Vegetation characteristics are presented in Table 2. Stem density was measured by counting the number of stems in a sample area of 0.5 m^2. This was repeated at up to 10 different locations. At each location, stem diameter was measured at the channel middepth for at least 40 randomly chosen stems, using digital Vernier gauge callipers. As *Carex* leaves are blade shaped, both width and thickness were recorded. Assuming orientation could be in any direction to the flow, the average of width and thickness was used for diameter. Both live and dead stems were included in the vegetation characterization. Solid volume fraction was estimated as $\phi=\pi 4^{-1}Nd^2$ and frontal facing area as $a=Nd$. Large uncertainties in ϕ are therefore due to the large variations in N and uncertainties in d.

Stem diameter and frontal facing area were also measured from images of the vegetation taken in front of a clear white board, with each cross-sectional image capturing 0.2 m longitudinally of vegetation for *Typha* and 0.05 m of vegetation for *Carex*. Separate estimates of d, a, and ϕ are presented based on the image processing. Unless otherwise specified, values of d obtained by calliper (and estimates of a and ϕ based on them) have been used in the data analysis presented here to remain consistent with other studies (Table 1).

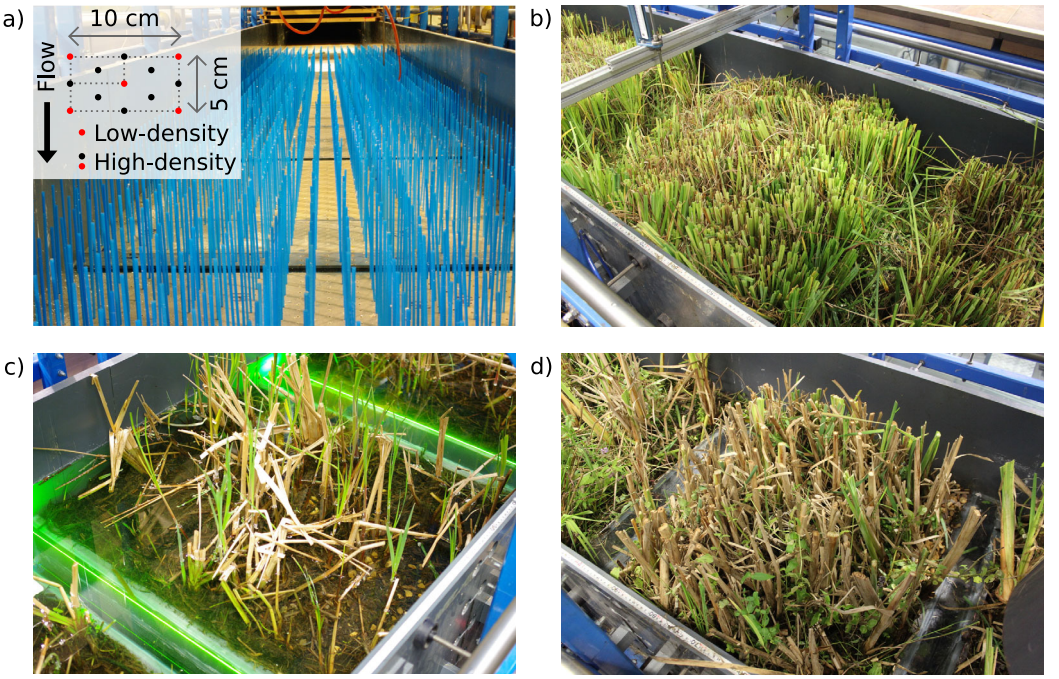

Figure 2. Photos of (a) low-density artificial vegetation, (b) *Carex*, (c) winter *Typha*, and (d) summer *Typha*. Inset (a) shows diagram of artificial vegetation.

Data were collected at flow rates of Q=1.0, 1.5, 2.0, 2.5, and 3.0 L s^{-1} with a flow depth of 0.15 m. A single 1 m long patch of vegetation was tested with 10 repeat injections at each flow rate. Although tests on additional vegetation patches would be desirable to reflect field scale variation, this was not feasible due to practical constraints. Within vegetated mixing, the relevant length scale for Reynolds number is typically stem diameter, $Re_d = Ud\nu^{-1}$. The collected data covers stem Reynolds numbers of $27 \leq Re_d \leq 524$, with the majority of tests falling below $Re_d = 200$, i.e., in the nominally laminar and transitional zones [*Nepf*, 1999]. Uncertainties in data from the studies presented in Table 1 have been included where possible.

3.3. Calculating Dispersion Coefficients

Similar to the *Fischer et al*. [1979] routing solution to the one-dimensional ADE, *Baek et al*. [2006] presented a routing solution for the two-dimensional ADE, varying in time longitudinally and transversely:

$$\hat{C}(x_2, y, t) = \int_{-\infty}^{\infty}\int_{-\infty}^{\infty} \frac{C(x_1, \lambda, \tau)U}{4\pi\bar{t}\sqrt{D_x D_y}} \exp\left(-\frac{U^2(\bar{t}-t+\tau)^2}{4D_x\bar{t}} - \frac{(y+\lambda)^2}{4D_y\bar{t}}\right) d\lambda\, d\tau \tag{11}$$

Table 2. Experimental Emergent Vegetation Characteristics from Present Study

Type[a]	Stem Density[c] N (stems/m^2)	Stem Diameter[d] d (m)	Frontal Facing Area[d] a (m^{-1})	Solid Volume Fraction[d] ϕ (–)	Stem Reynolds Re_d (–)
Hexagonal Low-density AV	398	0.004	1.592	0.005	27–82
Hexagonal High-density AV	1594	0.004	6.376	0.02	29–83
Summer *Carex acutiformis*	3388 ± 819	0.005 ± 0.001 0.006 ± 0.002[b]	18.3 ± 5.9 13.0 ± 3.8[b]	0.077 ± 0.03 0.060 ± 0.03[b]	32–82
Winter *Typha latifolia*	161 ± 72	0.010 ± 0.007 0.006 ± 0.005[b]	1.6 ± 1.4 2.5 ± 0.8[b]	0.013 ± 0.01 0.012 ± 0.01[b]	82–232
Summer *Typha latifolia*	171 ± 42	0.019 ± 0.010 0.015 ± 0.012[b]	3.2 ± 1.8 3.8 ± 0.7[b]	0.047 ± 0.04 0.045 ± 0.04[b]	178–524

[a]AV = artificial vegetation.
[b]Value based on image processing.
[c]Errors reflect spatial variation.
[d]Errors reflect uncertainty in the mean measurement.

where $\hat{C}$ is the routed or predicted concentration profile, $\bar{t}$ is the mean travel time, and τ and λ are the integration variables. In a routing or convolution solution to the ADE, each discretization of the upstream concentration profile is independently advected and dispersed downstream. The downstream concentration profile is the sum or superposition of the resulting individual profiles. This allows a prediction of the downstream concentration profile based on an upstream profile provided that U, D_x, D_y, and $\bar{t}$ are known. The routing solution uses the "frozen-cloud approximation" ($x = Ut$) in the longitudinal direction, i.e., assuming that no dispersion occurs during measurement or that $C(x_i, t) \cong C(x, t_i)$ [*Fischer et al.*, 1979].

An optimization approach has been taken to simultaneously obtain best fit values of transverse and longitudinal dispersion to the experimental data using the MATLAB nonlinear optimization function fmincon [*The MathWorks Inc.*, 2015]. This maximizes the goodness of fit between a downstream record and a downstream prediction by simultaneously varying D_x, D_y, U, and V (the temporal mean, transverse velocity). When optimizing, the transverse mean velocity V has been added (replacing y in the right-hand side of equation (11) with $y - V\bar{t}$) as a dummy variable to account for any 3-D flow field effects and to ensure that the spread of solute is accurately reflected. $\bar{t}$ was taken as the distance between measurement points (1 m) over longitudinal velocity, i.e., $\bar{t} = U^{-1}$. Goodness of fit was determined using a 2-D formulation of the *Young et al.* [1980] R_t^2:

$$R_t^2(C, \hat{C}) = 1 - \frac{\int_{-\infty}^{\infty}\int_{-\infty}^{\infty}\left(\hat{C}(x_2, \lambda, \tau) - C(x_2, \lambda, \tau)\right)^2 d\lambda\, d\tau}{\int_{-\infty}^{\infty}\int_{-\infty}^{\infty} C(x_2, \lambda, \tau)^2 d\lambda\, d\tau} \tag{12}$$

R_t^2 has been shown to be a robust means of evaluating the similarity of two temporal concentration profiles in optimization [*Sonnenwald et al.*, 2013]. Error in optimized D_x and D_y was estimated from the mean increase or decrease in value needed to cause a 5% reduction in R_t^2 [after *Lightbody and Nepf*, 2006b]. However, it is worth noting that R_t^2 is relatively insensitive to changes in either transverse or longitudinal dispersion coefficient.

The continuous injection data have been used to validate the 2-D pulse data collection and the 2-D optimization approach. The continuous injection data were temporally averaged and mass-balanced, resulting in two transverse concentration distributions. A downstream prediction was then optimized using a transverse version of the 1-D routing solution [*Fischer et al.*, 1979].

4. Results

4.1. Validation of the 2-D Routing Equation

Figure 3 shows an example upstream, downstream, and routed concentration distribution for one artificial and one real emergent vegetation test case. In the artificial vegetation, both the upstream and downstream distributions are close to Gaussian and there is relatively little spread (allowing both profiles to be shown on the same axes). In contrast, the real vegetation has upstream and downstream profiles that are asymmetric, reflecting the naturally more random spatial variation of the real vegetation. These morphological differences in the vegetation make it more difficult to characterize mixing, as evidenced by the lower R_t^2 in the real vegetation case. Mean R_t^2 was found to be 0.9346 with a standard deviation of 0.0598 in the artificial vegetation, compared with 0.7427 and 0.1151 in the real vegetation. The lower quality of the fit of the tail for the real vegetation, e.g., Figure 3c, suggests that the Gaussian transfer function assumption implicit in the use the ADE equation may not be entirely suitable.

Continuous injection data for the *Typha* and high-density artificial vegetation were used to validate the application of the 2-D routing equation for obtaining dispersion coefficients from pulse injection data. Figure 4 presents a comparison of D_y optimized from both the continuous and pulse injection data. As it is not possible to optimize for longitudinal velocity from transverse continuous concentration records, an estimate of velocity based on number of stems and stem diameter, $U = QA^{-1}[(1 - \sqrt{N}d + Nd^2)/(1 - \sqrt{N}d)]$, where A is empty flume cross-sectional area, has been used instead. Ideally, recorded velocity data would be used here, but it was not of sufficient quality in this case due to difficulties with the probes at low velocities. The velocities differ due to the continuous injection velocity estimate not accounting for vegetation layout and

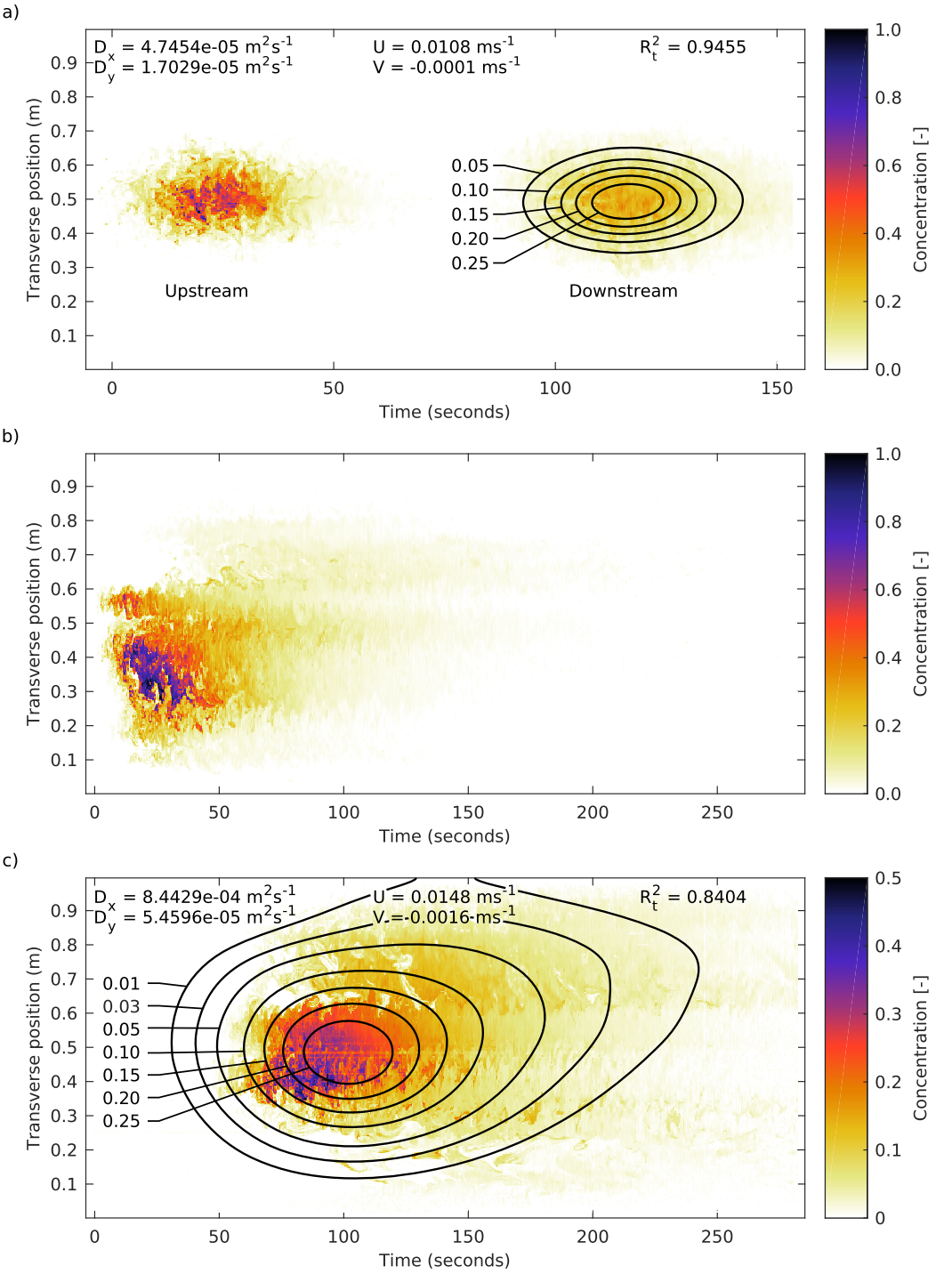

Figure 3. Example (a) upstream and downstream concentration profiles for artificial vegetation, (b) upstream concentration profile for real vegetation, and (c) downstream concentration profile for real vegetation. Contours show downstream prediction using optimized values in equation (11).

other 3-D flow complexities. The estimate is closest to the optimized velocities for the artificial vegetation, which has the simplest geometry.

For both the high-density artificial vegetation and the winter *Typha* vegetation, there is good agreement between D_y from the continuous and the pulse injections. Agreement for the summer *Typha* is not as good.

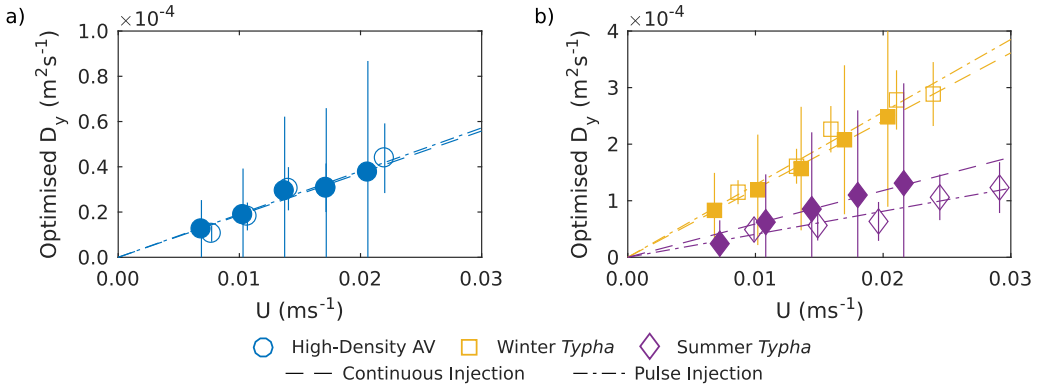

Figure 4. Comparison of transverse dispersion recorded from continuous and pulse injections with linear trend lines for (a) high-density artificial vegetation and (b) *Typha*. Solid symbols represent continuous injection data, open symbols the pulse injection data.

The difference between the pulse and continuous optimized results is likely to be the result of a more complex interaction between D_x and D_y that is captured only in a full 2-D routing optimization. The large error bars on the continuous injection values are the result of taking an optimized value from a single injection. Overall, the comparison confirms that the 2-D ADE routing equation can be used to form reasonable bulk scale estimates of dispersion coefficients for emergent vegetation.

4.2. Results From the 2-D Routing Analysis

Figure 5 shows the mean optimized transverse and longitudinal dispersion coefficients obtained from 2-D optimization of the pulse injection data. The expected trend of increasing dispersion with velocity is clearly shown [*Fischer et al.*, 1979].

Figures 5a and 5b show only a slight difference in dispersion for the two densities of artificial vegetation. Longitudinal dispersion is approximately two-and-a-half times greater than transverse dispersion. The low-density artificial vegetation shows slightly greater transverse dispersion compared with the high-density artificial vegetation, whereas longitudinal dispersion within the two is nearly identical. Dimensionless dispersion, $D(Ud)^{-1}$ (Figures 5c and 5d) is constant within error bars for both D_x and D_y, confirming a linear relationship with U. The similarity of dispersion coefficients for the two types of artificial vegetation suggests that the similar pattern of the stems at the two densities is playing an important role in controlling dispersion.

Figures 5e and 5f show dispersion within the real vegetation, which is greater than that within the artificial vegetation by an order of magnitude. *Carex* and summer *Typha* have very different physical characterizations, yet show similar values of transverse dispersion. Winter *Typha*, which is similar in characterization to summer *Typha*, shows much greater transverse dispersion. Longitudinal dispersion varies between all three vegetation types, increasing with solid volume fraction. The greater values and variability of dispersion for the real vegetation reflect the increased complexity of the flow field. It may be seen from Figure 2 that winter *Typha* is less uniform with greater stem spacings than summer *Typha* which also has larger stems ($d = 0.010$, cf. $d = 0.019$ m) and is denser (ϕ=0.047, cf. ϕ=0.013 m). *Carex* appears to be much more uniform than the *Typha* and is also more dense with ϕ=0.077. Winter and summer *Typha* both show optimized mean longitudinal velocities for the same flow rate consistent with the increase in solid volume fraction between the two (visible as spread on x axis coordinates of Figures 5e–5h). *Carex*, despite having a solid volume fraction greater than summer *Typha*, has a lower optimized mean velocity. This may be due to the high number of stems ($N = 3388$) increasing the length of the flow path.

Figures 5g and 5h show dimensionless optimized dispersion coefficients for the real vegetation. In the absence of other data, no systematic variation and a single constant value of dimensionless dispersion for each vegetation type would be expected. Winter and summer *Typha* show near constant values of $D(Ud)^{-1}$, but the *Carex* results show more scatter, with two points clearly not fitting a horizontal (constant) line. Winter *Typha* and *Carex* share a constant value of transverse dispersion within error, as do summer and winter *Typha* for longitudinal dispersion. Dimensionless dispersion is different for all three

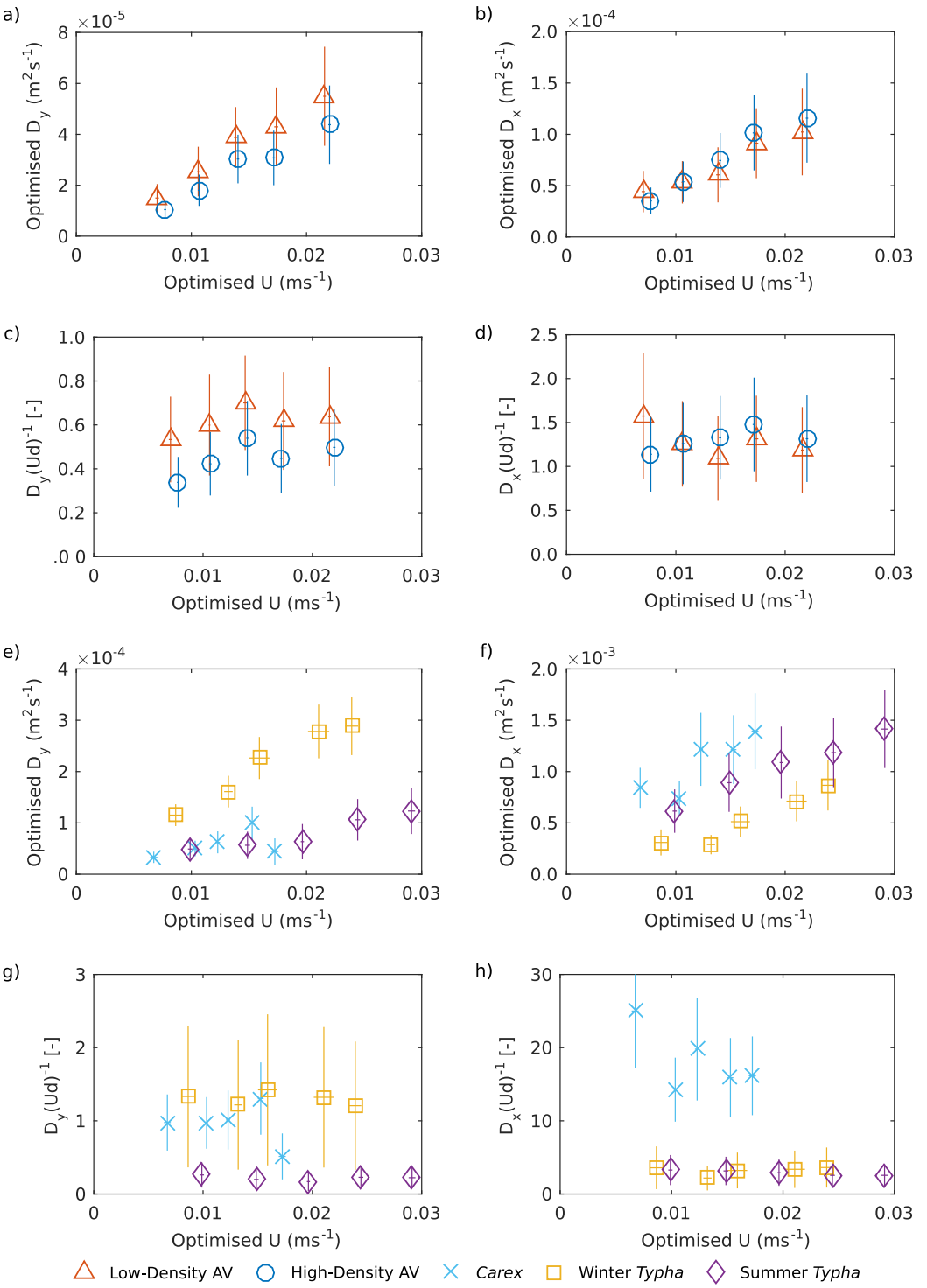

Figure 5. Mean optimized (left) transverse and (right) longitudinal dispersion coefficients and dimensionless dispersion coefficients for: (a), (b), (c) and (d) artificial vegetation; (e), (f), (g), and (h) real vegetation.

vegetation types, which demonstrates the influence of their different vegetation characteristics, such as solid volume fraction. While no measurement of bed roughness has been calculated, visual inspection suggests that bed level may vary on the order of 0.01–0.02 m. Any differences in bed morphology between the vegetation types that may affect dispersion are not accounted for when nondimensionalizing by stem diameter.

5. Discussion

5.1. Comparison With Other Data and Models

Figure 6 compares the new dispersion data with the data outlined in Table 1, plotted as a function of solid volume fraction, ϕ. Figure 6 demonstrates both the breadth of the available data and the variability in results. Dimensionless longitudinal dispersion is typically an order of magnitude greater than transverse dispersion. The transverse dispersion data does not suggest a dependency on ϕ, whereas there is some indication of an inverse trend between longitudinal dispersion and solid volume fraction.

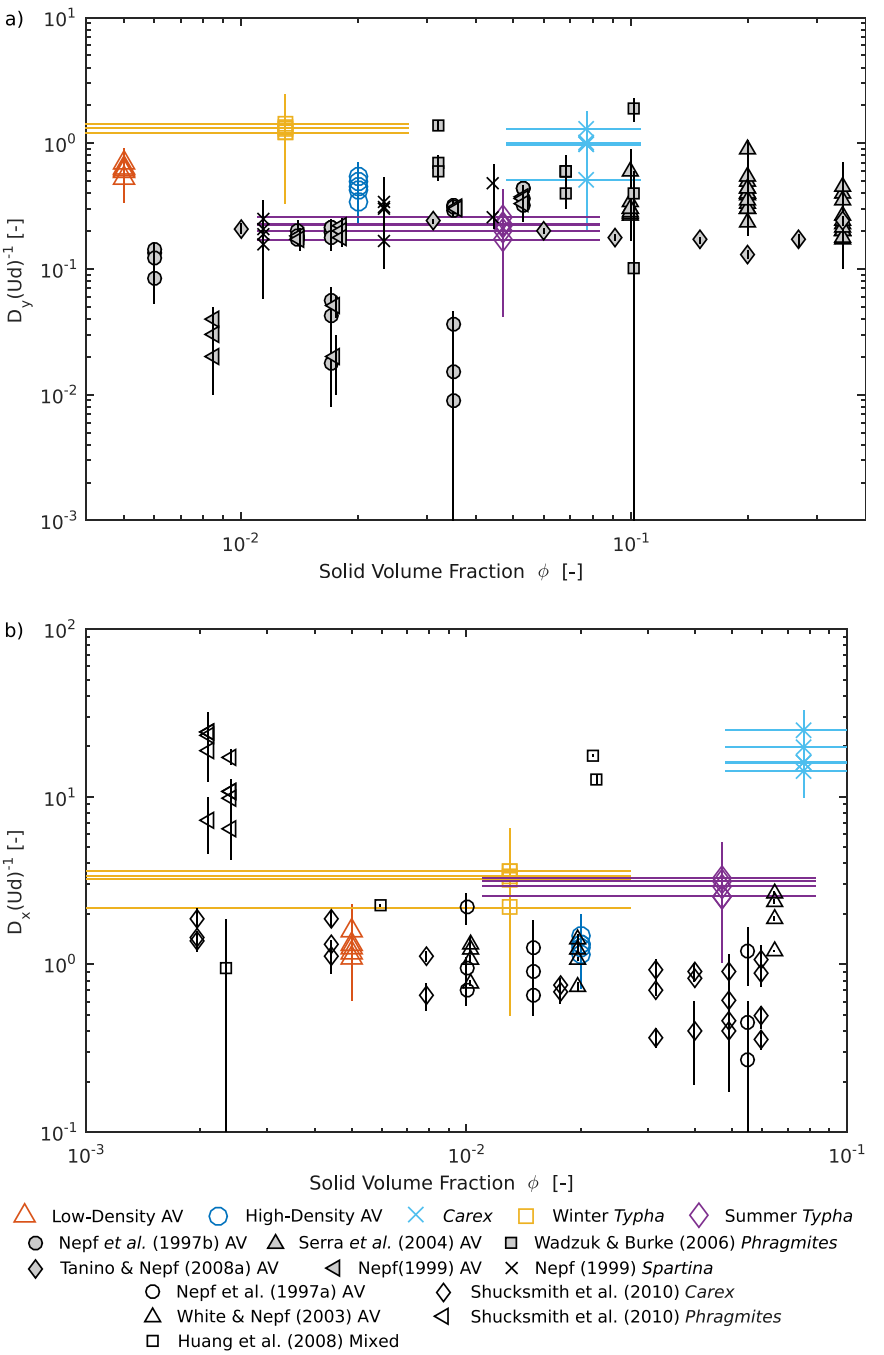

Figure 6. Combined plots of experimental values of (a) dimensionless transverse dispersion $D_y(Ud)^{-1}$ and (b) dimensionless longitudinal dispersion $D_x(Ud)^{-1}$ from the new and the other data sets outlined in Table 1.

5.2. Transverse Dispersion

5.2.1. Artificial Vegetation

The high-density artificial vegetation behaves very similarly to the low-density artificial vegetation, with slightly reduced transverse dispersion (Figure 5a). This is at odds with the *Nepf* [1999] mixing model. *Nepf* [2012] suggested that at $\phi < 0.1$ transverse mixing is dominated by turbulent processes and so, from the first term of equation (2) and $ad \approx \phi$, the high-density artificial vegetation would be predicted to have 1.6 times greater transverse dispersion than the low-density artificial vegetation. However, in this case, substituting in $Dy(Ud)^{-1}$ values for high and low-density artificial vegetation respectively, the ratio is instead $0.45/0.62 = 0.73$. *Guo et al.* [2014] created a numerical model for periodic arrays of cylinders and showed, consistent with this result, that longitudinal and transverse dispersion increased with decreasing solid volume fraction in a diamond array of vegetation.

It is likely that periodic artificial vegetation presents a special case compared to random artificial vegetation due to the development of a periodic velocity field [*Meftah and Mossa*, 2013; *West*, 2016]. Visual inspection of the dye traces within the artificial vegetation, not shown, show clear repeating variations in dye concentration that meander back and forth. The repeating variations can be shown to correlate with stem spacing, suggesting that stem spacing—rather than stem diameter—is the dominant length scale. If stem-spacing instead of diameter is used to nondimensionalize the artificial vegetation, i.e., $D_y(Us)^{-1}$, then the ratio of high-density to low-density dispersion becomes $0.07/0.05 = 1.4$. This is consistent with *Nepf* [1999], demonstrating that stem-spacing is the appropriate length scale.

The repeating variations in dye concentration suggest large coherent flow structures. The regularity of the observed flow structures is only possible within periodic arrays of artificial vegetation, since within random vegetation the positioning of stems ensures that such structures are broken down. The stem spacing length scale in the artificial vegetation here is inconsistent with the results of *Tanino and Nepf* [2008a], who showed that stem spacing as the dominant length scale occurs at much greater solid volume fractions ($\phi > 0.1$) than seen here. It follows that periodic arrays of cylinders are not representative of real vegetation for dispersion analysis.

5.2.2. Transverse Mixing Model Comparisons With the New Real Vegetation Results

Figure 7 shows the *Nepf* [1999], *Tanino and Nepf* [2008a], and *Nepf* [2012] predictions of dimensionless transverse dispersion against ϕ. A value of $C_D = 1$ has been assumed within equation (2). The *Tanino and*

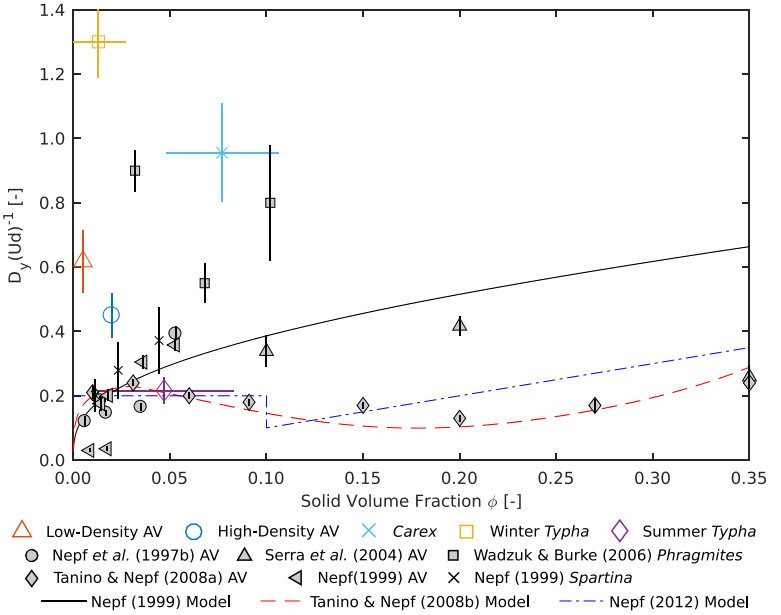

Figure 7. Comparison of experimental values of dimensionless transverse dispersion $D_y(Ud)^{-1}$ from new data (open symbols) and other data sets (filled symbols, outlined in Table 1) with existing models (lines).

Nepf [2008a] model is a modification of the *Nepf* [1999] model such that the drag force energy dissipation component decreases at higher solid volume fractions. *Nepf* [2012] suggested that $D_y(Ud)^{-1}=0.2$ may be used to predict transverse dispersion in emergent vegetation when $\phi < 0.1$ and that $D_y(Ud)^{-1} \approx \phi$ when $\phi \geq 0.1$.

It is immediately apparent that none of the models is capable of predicting the high levels of dimensionless transverse dispersion associated with the *Wadzuk and Burke* [2006] *Phragmites* data or the new winter *Typha* or *Carex* data. With real vegetation, only dispersion for the summer *Typha* and the *Nepf* [1999] *Spartina* fall close to any of the model predictions. Assuming drag force energy dissipation as the dominant mechanism, the enhanced dispersion values in real vegetation suggest that more energy dissipation is occurring than the models predict. Given its high stem density and decreased optimized velocities (increased mean travel times) the Carex may instead be experiencing enhanced flow path tortuosity. The scatter in the data for real vegetation implies that the models all omit some key mixing processes. *Burke and Wadzuk* [2009] suggests that these processes could be pockets of turbulence and dead zones, and that accounting for these within the *Wadzuk and Burke* [2006] data makes the data more consistent with the existing models. Dead zone effects could also account for the previously discussed lower optimized mean velocities of the *Carex*.

5.3. Longitudinal Dispersion

5.3.1. Artificial Vegetation

Similar to transverse dispersion, there is almost no difference in longitudinal dispersion between the two densities of artificial vegetation (Figure 5b). However, while a difference in D_y would be expected, it is less clear that a difference in D_x is expected. *White and Nepf* [2003] suggested that longitudinal dispersion due to vortex trapping may change with *ad*, but that vortex trapping is also heavily influenced by terms dependent on Re_d, which remains the same between densities. Similarly, according to *Lightbody and Nepf* [2006b], secondary wake dispersion is dependent on C_D, which is again dependent on Re_d.

5.3.2. Longitudinal Mixing Model Comparisons With the New Real Vegetation Results

Figures 8a and 8b show predictions of the vortex trapping and secondary wake terms of the *White and Nepf* [2003] longitudinal dispersion model, respectively, compared to a line of equality. For the vortex trapping term, $D_{x,t}$, the model parameters $\beta_w=2.25$, $\kappa_w=1$, and $St=0.2$ have been used, based on the values given by *White and Nepf* [2003]. The simplified secondary wake dispersion term, equation (8), provided by *Lightbody and Nepf* [2006b] has been used. Typically, drag coefficient can be obtained experimentally by measuring a change in head before and after the vegetation [*Nepf*, 1999]. However, due to the low velocities within the flume, its horizontal bed, and the resolution of the available instrumentation, it was not possible to measure a change in head. Drag has, therefore, been estimated from the results of

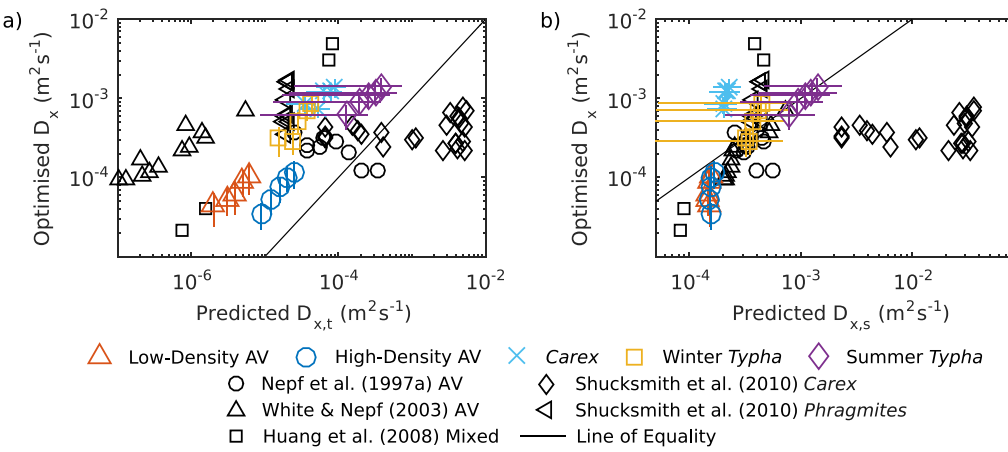

Figure 8. Longitudinal mixing model predictions for the *White and Nepf* [2003] (a) vortex trapping and (b) secondary wake dispersion mechanisms. *x* axis shows predictions and *y* axis shows observed dispersion.

Tanino and Nepf [2008b] and *Tinoco and Cowen* [2013], who both utilized an expression derived from *Ergun* [1952]:

$$C_D = 2\left(\frac{\alpha_0}{Re_d} + \alpha_1\right) \tag{13}$$

where α_0 and α_1 are parameters dependent on the vegetation. Their experimental results combined produce the empirical best fit relationships:

$$\begin{aligned} \alpha_0 &= 7276.43d + 23.55 \\ \alpha_1 &= 32.70d + 3.01\phi + 0.42 \end{aligned} \tag{14}$$

which have been used in equation (13) to estimate C_D. The experimental work did not provide sufficient evidence of vertical heterogeneity to support the application of the *Lightbody and Nepf* [2006a, 2006b] models. This is not surprising as the shallow flow depth of 0.15 m here is expected to minimize the effects due to vertical shear.

Similar to results presented in *White and Nepf* [2003], $D_{x,t}$ is several times smaller than $D_{x,s}$. The vortex trapping mechanism on its own is insufficient to predict longitudinal mixing (Figure 8a); this is consistent with *Lightbody and Nepf* [2006a] subsequently ignoring the vortex trapping component of longitudinal dispersion. The secondary wake dispersion mechanism provides a much better predictor (Figure 8b), with summer *Typha* falling on the line of equality. The error bars in the winter *Typha* prediction almost all include the line of equality. However, the model under-predicts dispersion within the *Carex*. The inclusion of the vortex trapping mechanism in the *White and Nepf* [2003] model does not significantly change the quality of the predictions; the plot is visually indistinguishable from Figure 8b.

While the *White and Nepf* [2003] model predicts their own data well, and some of the *Nepf et al*. [1997a] and *Shucksmith et al*. [2010] *Phragmites* data reasonably well, dispersion due to the new artificial vegetation is over-estimated. The *Huang et al*. [2008] data are either over-estimated or under-estimated and the *Shucksmith et al*. [2010] *Carex* data over-estimated. The latter may reflect the high Reynolds numbers associated with this particular test series, but it should also be noted that the predicted values are highly sensitive to the estimated C_D values such that any error in the laboratory quantification of d or ϕ may have a substantial impact on the modeled value of $D_{x,s}$.

5.4. Seasonal Variation in Real Vegetation

Through the growing seasons of spring and summer, vegetation becomes denser and stems thicken before dying back during the winter [*O'Hare*, 2015]. The winter *Typha* is irregular, and stems exist at odd angles and in clumps. In comparison, summer *Typha* has stems approximately twice as thick with three times the solid volume fraction. The *Nepf* [1999] (equation (2)) and *Tanino and Nepf* [2008a] (equation (5)) transverse dispersion models suggest that the summer *Typha* vegetation would result in greater dimensionless transverse dispersion than winter *Typha*. Figure 5g shows the reverse. Dimensionless longitudinal dispersion (Figure 5h) shows minimal seasonal dependency. Given the differences in vegetation characterization, none of the longitudinal mixing models predict this.

The *Carex* vegetation is from the summer season. *Shucksmith et al*. [2010] showed *Carex* increasing in density with growth (age), but exhibiting relatively constant longitudinal dispersion, suggesting that winter *Carex* would perform similarly to the results presented for summer *Carex*. This is consistent with the *Typha* data presented here. *Valiela et al*. [1975] showed quite significant variation in biomass through a season for salt marsh vegetation. *Karunaratne et al*. [2003], however, showed that seasonal variation of vegetation could be minimal in some cases. These observations suggest that additional investigation into seasonal variation is necessary.

The seasonal differences in dimensionless transverse dispersion of *Typha* are greater than their measured physical characteristics would indicate suggesting that some additional characteristic is of importance. The clustering of stems in winter *Typha* is potentially affecting dispersion, either causing them to act as single, larger, obstacle, or by trapping flow within the clusters. *Burke and Wadzuk* [2009] suggest that a similar clustering of *Phragmites australis* stems affects the results of *Wadzuk and Burke* [2006]. Alternatively, more open areas in winter *Typha* may increase bed-generated shear components of dispersion. Such effects are

ignored when nondimensionalizing solely by stem diameter. Ideally tests of additional 1 m patches of winter *Typha* would be carried out to better isolate any of these effects.

5.5. Characterizing Real Vegetation

Although several of the evaluated models provide reasonable estimates of dispersion within artificial vegetation, dispersion within real vegetation is generally poorly predicted. There are three main vegetation characteristics used within the models: solid volume fraction, frontal facing area, and stem diameter. The first two are bulk properties. Stem diameter, d, however, is a mean value, which is sensitive to variations in individual stem properties. Measurements of d taken by hand compared to those obtained from image analysis (Table 2) are similar, but do not coincide exactly. However, a large spread of values was observed in both cases. Despite the natural variability of d, all analysis performed within this paper has used a single value of mean stem diameter. The uncertainty in d is apparent in the large vertical error bars when observed dispersion is nondimensionalized. *Wadzuk and Burke* [2006] report a similarly high level of variability in stem diameter to the *Typha* with $d=0.0152\pm0.011$ m ranging from 0.004 to 0.042 m [*Burke and Wadzuk*, 2009], while *Nepf* [1999] reported little variability with $d=0.0069\pm0.0003$ m.

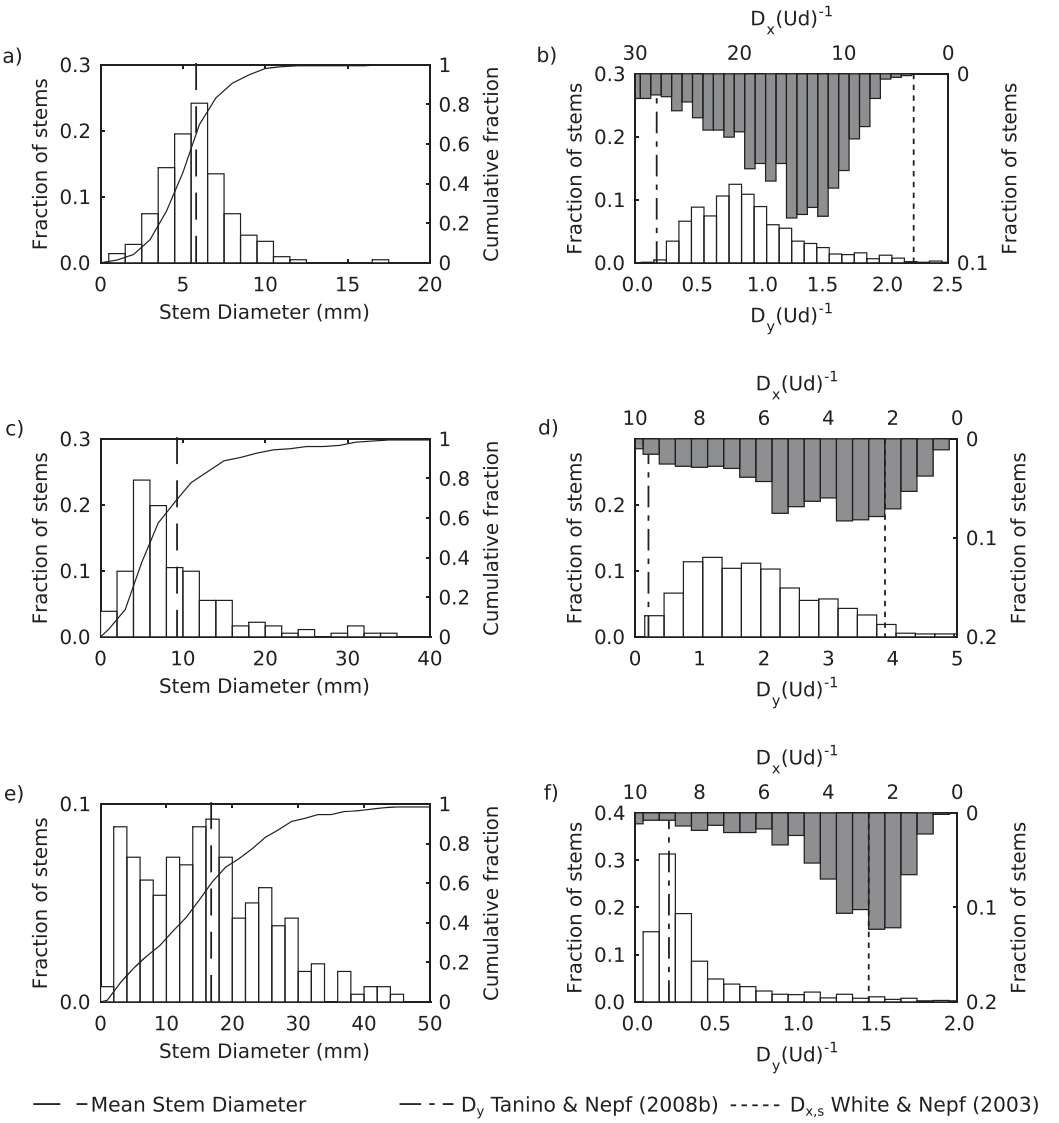

Figure 9. (a) and (b) *Carex*, (c) and (d) winter *Typha*, and (e) and (f) summer *Typha* distributions of (left) stem diameters and (right) dimensionless dispersion with *Tanino and Nepf* [2008a] and *White and Nepf* [2003] secondary wake model predictions as dashed vertical lines in Figures 9b, 9d, and 9f.

Figure 9 (left column) shows the distribution of measured stem diameters for each of the three types of real vegetation. In this case, the measurements made using callipers and those derived from photographic image processing have been combined. For all three types of vegetation, the stem diameter distribution is skewed and the mean is larger than the median (d_{50}) of the distribution. The mode (peak) of the distribution for winter *Typha* is less than the mean, while the mode and the mean are approximately the same for the summer *Typha* and *Carex* distributions. The distributions of both winter *Typha* and *Carex* exhibit a clear single peak, while the summer *Typha* appears to have two peaks, one close to the mean diameter at around 0.017 m and a second at around 0.002 m.

Figure 9 (right column) shows the effect of nondimensionalizing the observed values of D_x and D_y using the stem diameter distributions instead of the single mean stem diameter. Here the mean values of optimized D_x and D_y, as presented in Figure 5, have been used for nondimensionalization. In each case, the distributions are skewed, and show considerable spread around the mean values of nondimensional dispersion presented in Figures 5g and 5h, i.e., $D_y(Ud)^{-1}$ values of ~1.0, 1.3, and 0.2 and $D_x(Ud)^{-1}$ values of ~18, 3, and 3 for *Carex*, winter *Typha* and summer *Typha*, respectively. The greatest spread is in the dimensionless longitudinal dispersion for *Carex* (Figure 9b), which varies from approximately zero to more than 30 depending on whether the largest or smallest observed stem diameter is assumed.

Figure 9 (right column) also presents dimensionless transverse dispersion as predicted by *Tanino and Nepf* [2008a] and secondary wake longitudinal dispersion as predicted by *White and Nepf* [2003]. These values have been presented earlier in this paper, and are all based on the mean stem diameter from calliper measurements. As has already been shown, the *Tanino and Nepf* [2008a] model provides a good estimate of the nondimensional transverse dispersion for the summer *Typha*, but significantly underestimates the observed transverse dispersion for *Carex* and winter *Typha*. The *White and Nepf* [2003] model provides a reasonable estimate of nondimensional longitudinal dispersion for both winter and summer *Typha*, but an underestimate for *Carex*.

Given the skewed nature of the stem diameter distributions, it may be argued that the peak (mode) or d_{50} (median) values should provide a more representative average compared with the geometric mean. Nondimensionalizing the observed values of dispersion using either of these (smaller) stem diameters would, however, act to increase $D(Ud)^{-1}$, tending to move the observed data further away from the existing model predictions. Alternatively, there may be some justification for using d_{90}, the value representing the diameters of the largest 10% of stems, as it is often the larger length scales that dominate dispersion. If $d_{90} > d$ then d_{90} acts to reduce $D(Ud)^{-1}$, in this case by approximately a factor of two. This does not significantly bring the experimental results more in line with model predictions.

These observations suggest either that the existing models are unable to capture the complex mixing processes that characterize real, heterogeneous, vegetation, or that the relevant length scale is not stem diameter. For winter *Typha*, Figure 2c shows clusters of stems that could effectively be acting as a single larger stem. Conversely, while the modeled dispersion for summer *Typha* provides a good estimate of the observed data, it is evident that stems with diameters lower than the mean diameter appear with equal frequency to the mean diameter. These smaller diameter stems must therefore have an equal contribution to mixing, but are ignored in any estimates based on mean stem diameter alone. The models for both transverse and longitudinal dispersion under estimate dispersion for *Carex*. While this is also the case with the winter *Typha*, it cannot be due to the same reasons as they have dissimilar morphology. While winter *Typha* is quite patchy, Figure 2b shows the *Carex* appears quite dense. Visual inspection of dye traces through the *Carex* show a very long tail indicating significant dye-trapping within the vegetation. This longitudinal dispersion mechanism is not well accounted for in any of the models. *Tanino and Nepf* [2008a] included the distribution of stem spacings as a key mixing-length control within their model for transverse dispersion. The data presented here suggests that the predictions of both longitudinal and transverse dispersion within real emergent vegetation may require the variability in stem diameter and stem clustering to be considered alongside the variation in stem spacing.

5.6. Modeling Recommendations

The new data for dispersion in real emergent vegetation is not predicted satisfactorily by any of the existing models. The scatter and uncertainty in modeling the available data suggests that for design purposes it may be appropriate to adopt the vegetation (and season)-specific parameter values, as presented in Figures

5e and 5f. *O'Hare* [2015] has suggested the application of plant morphogroups (plant grouping based on physical characteristics) to hydrodynamic modeling, and this approach could prove suitable for simplifying the task of choosing species and characterizations for modeling in the future.

6. Conclusions

A new data set has been presented that, for the first time, simultaneously describes transverse and longitudinal dispersion in both artificial and real emergent vegetation. Within periodic artificial vegetation, a regular velocity field develops that make it unsuitable for simulating real vegetation. Dispersion within the real vegetation is complex and shows differences between the two species (*Carex acutiformis* and *Typha latifolia*) and two seasons (winter and summer *Typha*). Dispersion has been nondimensionalized by mean stem diameter, and *Carex* shows significantly greater dimensionless longitudinal dispersion, compared with the other two ($D_x(Ud)^{-1} \approx 18$ versus $D_x(Ud)^{-1} \approx 3$). *Carex* and winter *Typha* have similar dimensionless transverse dispersion ($D_y(Ud)^{-1} \approx 1.0$), while summer *Typha* shows much less dimensionless transverse dispersion ($D_y(Ud)^{-1} \approx 0.2$).

The new emergent vegetation mixing data have been combined with other previously published results and the combined data set compared with models for predicting dispersion in emergent vegetation. The data set shows significant scatter compared to model predictions. The *Nepf* [2012] transverse mixing model and *White and Nepf* [2003] longitudinal mixing model currently offer the closest predictions of dispersion coefficient, but much of the new and existing data is not predicted well.

The lack of predictive capability of the existing emergent vegetation dispersion models and the variability of the available dispersion data highlights that real vegetation is a complex and highly variable natural material. The results suggest that relying on mean diameter to describe mixing length scales fails to fully characterize the vegetation, and that future research should focus on developing models that can fully capture the distribution of mixing length scales and the associated mixing processes.

Acknowledgments
This work was supported by the Engineering and Physical Sciences Research Council. (EPSRC grants EP/K024442/1, EP/K025589/1). The experimental work would not have been possible without the expert technical support of Ian Baylis. The authors are grateful to Dr. James Shucksmith for access to experimental data used in this research and to Professor Heidi Nepf for useful discussions on dispersion within real vegetation. The authors thank the reviewers for their positive and thorough feedback. The data in this work are based on will be available from http://vpond.group.shef.ac.uk/.

References

Baek, K. O., I. W. Seo, and S. J. Jeong (2006), Evaluation of dispersion coefficients in meandering channels from transient tracer tests, *J. Hydraul. Eng.*, *132*(10), 1021–1032.
Burke, E. N., and B. M. Wadzuk (2009), The effect of field conditions on low Reynolds number flow in a wetland, *Water Res.*, *43*(2), 508–514.
Ergun, S. (1952), Fluid flow through packed columns, *Chem. Eng. Prog.*, *48*, 89–94.
Erqing, H., C. Guangjing, J. Chunbo, and Z. Zhenduo (2010), Longitudinal dispersion of pollutants in flow through natural vegetation, in *2010 4th International Conference on Bioinformatics and Biomedical Engineering (iCBBE)*, pp. 1–6, IEEE, New York.
Ferrier, A., D. Funk, and P. Roberts (1993), Application of optical techniques to the study of plumes in stratified fluids, *Dyn. Atmos. Oceans*, *20*(1), 155–183.
Fischer, H. B., J. E. List, C. R. Koh, J. Imberger, and N. H. Brooks (1979), *Mixing in Inland and Coastal Waters*, Elsevier., San Diego, Calif.
Goring, D. G., and V. I. Nikora (2002), Despiking acoustic Doppler velocimeter data, *J. Hydraul. Eng.*, *128*(1), 117–126.
Guo, X., B. Wang, and C. C. Mei (2014), Flow and solute transport through a periodic array of vertical cylinders in shallow water, *J. Fluid Mech.*, *756*, 903–934.
Huang, Y. H., J. E. Saiers, J. W. Harvey, G. B. Noe, and S. Mylon (2008), Advection, dispersion, and filtration of fine particles within emergent vegetation of the Florida everglades, *Water Resour. Res.*, *44*, W04408, doi:10.1029/2007WR006290.
Karunaratne, S., T. Asaeda, and K. Yutani (2003), Growth performance of *Phragmites australis* in Japan: Influence of geographic gradient, *Environ. Exp. Bot.*, *50*(1), 51–66.
Lightbody, A., and H. Nepf (2006a), Prediction of near-field shear dispersion in an emergent canopy with heterogeneous morphology, *Environ. Fluid Mech.*, *6*(5), 477–488.
Lightbody, A. F., and H. M. Nepf (2006b), Prediction of velocity profiles and longitudinal dispersion in emergent salt marsh vegetation, *Limnol. Oceanogr. Methods*, *51*(1), 218–228.
Meftah, M. B., and M. Mossa (2013), Prediction of channel flow characteristics through square arrays of emergent cylinders, *Phys. Fluids*, *25*(4), 045,102.
Merritt, D. M., and E. E. Wohl (2002), Processes governing hydrochory along rivers: Hydraulics, hydrology, and dispersal phenology, *Ecol. Appl.*, *12*(4), 1071–1087.
Murphy, E. (2006), Longitudinal dispersion in vegetated flow, PhD thesis, Mass. Inst. of Technol., Boston, Mass.
Nepf, H., C. Mugnier, and R. Zavistoski (1997a), The effects of vegetation on longitudinal dispersion, *Estuarine Coastal Shelf Sci.*, *44*(6), 675–684.
Nepf, H., J. Sullivan, and R. Zavistoski (1997b), A model for diffusion within emergent vegetation, *Limnol. Oceanogr.*, *42*(8), 1735–1745.
Nepf, H. M. (1999), Drag, turbulence, and diffusion in flow through emergent vegetation, *Water Resour. Res.*, *35*(2), 479–489.
Nepf, H. M. (2000), Reply to "comment on 'drag, turbulence, and diffusion in flow through emergent vegetation' by HM Nepf", *Water Resour. Res.*, *36*(7), 1987–1988.
Nepf, H. M. (2012), Flow and transport in regions with aquatic vegetation, *Annu. Rev. Fluid Mech.*, *44*, 123–142.
Nikora, V. (2000), Comment on "drag, turbulence, and diffusion in flow through emergent vegetation" by HM Nepf, *Water Resour. Res.*, *36*(7), 1985–1986.

Nishihara, G. N., and R. Terada (2010), Spatial variations in nutrient supply to the red algae *Eucheuma serra* (J. Agardh) J. Agardh, *Phycol. Res.*, *58*(1), 29–34.
O'Hare, M. T. (2015), Aquatic vegetation—A primer for hydrodynamic specialists, *J. Hydraul. Res.*, *53*(6), 687–698.
Serra, T., H. J. Fernando, and R. V. Rodríguez (2004), Effects of emergent vegetation on lateral diffusion in wetlands, *Water Res.*, *38*(1), 139–147.
Shilton, A. (2000), Potential application of computational fluid dynamics to pond design, *Water Sci. Technol.*, *42*(10), 327–334.
Shucksmith, J., J. Boxall, and I. Guymer (2010), Effects of emergent and submerged natural vegetation on longitudinal mixing in open channel flow, *Water Resour. Res.*, *46*, W04504, doi:10.1029/2008WR007657.
Sonnenwald, F., V. Stovin, and I. Guymer (2013), Correlation measures for solute transport model identification & evaluation, in *Experimental and Computational Solutions of Hydraulic Problems*, edited by P. Rowinski, Springer, New York.
Tanino, Y., and H. M. Nepf (2008a), Lateral dispersion in random cylinder arrays at high Reynolds number, *J. Fluid Mech.*, *600*, 339–371.
Tanino, Y., and H. M. Nepf (2008b), Laboratory investigation of mean drag in a random array of rigid, emergent cylinders, *J. Hydraul. Eng.*, *134*(1), 34–41.
The MathWorks Inc. (2015), *MATLAB R2015b*, Natick, Mass.
Tinoco, R. O., and E. A. Cowen (2013), The direct and indirect measurement of boundary stress and drag on individual and complex arrays of elements, *Exp. Fluids*, *54*(4), 1–16.
Valiela, I., J. M. Teal, and W. J. Sass (1975), Production and dynamics of salt marsh vegetation and the effects of experimental treatment with sewage sludge: Biomass, production and species composition, *J. Appl. Ecol.*, *12*, 973–981.
Wadzuk, B. M., and E. Burke (2006), A diffusion model for low Reynolds number flows through a constructed stormwater wetland, in *Proceedings of the 7th International Conference on HydroScience and Engineering*, Philadelphia, Pa.
West, P. (2016), Quantifying solute mixing and flow fields in low velocity emergent real vegetation, PhD thesis, Univ. of Warwick, Coventry, U. K.
White, B. L., and H. M. Nepf (2003), Scalar transport in random cylinder arrays at moderate Reynolds number, *J. Fluid Mech.*, *487*, 43–79.
Young, P., A. Jakeman, and R. McMurtrie (1980), An instrumental variable method for model order identification, *Automatica*, *16*(3), 281–294, doi:10.1016/0005-1098(80)90037-0.